The Astrophysical Journal, 711:1073–1086, 2010 March 10 doi:10.1088/0004-637X/711/2/1073

SPECTRAL LAGS AND THE LAG–LUMINOSITY RELATION: AN INVESTIGATION WITH *SWIFT* BAT GAMMA-RAY BURSTS

T. N. Ukwatta[1,2], M. Stamatikos[2,3,7], K. S. Dhuga[1], T. Sakamoto[2,4,5], S. D. Barthelmy[2], A. Eskandarian[1], N. Gehrels[2], L. C. Maximon[1], J. P. Norris[6], and W. C. Parke[1]
[1] George Washington University, Washington, DC 20052, USA
[2] NASA Goddard Space Flight Center, Greenbelt, MD 20771, USA
[3] Department of Physics, Ohio State University, 191 West Woodruff Avenue, Columbus, OH 43210, USA
[4] Center for Research and Exploration in Space Science and Technology (CRESST), NASA Goddard Space Flight Center, Greenbelt, MD 20771, USA
[5] University of Maryland, Baltimore County, Baltimore, MD 21250, USA
[6] Department of Physics and Astronomy, University of Denver, 2112 East Wesley Avenue, Room 211, Denver, CO 80208, USA
Received 2009 May 8; accepted 2010 January 27; published 2010 February 22

ABSTRACT

Spectral lag, the time difference between the arrival of high-energy and low-energy photons, is a common feature in gamma-ray bursts (GRBs). Norris et al. reported a correlation between the spectral lag and the isotropic peak luminosity of GRBs based on a limited sample. More recently, a number of authors have provided further support for this correlation using arbitrary energy bands of various instruments. In this paper, we report on a systematic extraction of spectral lags based on the largest *Swift* sample to date of 31 GRBs with measured redshifts. We extracted the spectral lags for all combinations of the standard *Swift* hard X-ray energy bands: 15–25 keV, 25–50 keV, 50–100 keV, and 100–200 keV and plotted the time dilation corrected lag as a function of isotropic peak luminosity. The mean value of the correlation coefficient for various channel combinations is -0.68 with a chance probability of $\sim 0.7 \times 10^{-3}$. In addition, the mean value of the power-law index is 1.4 ± 0.3. Hence, our study lends support to the existence of a lag–luminosity correlation, albeit with large scatter.

Key words: gamma-ray burst: general

Online-only material: color figures

1. INTRODUCTION

After decades of research, a satisfactory explanation of the temporal behavior of gamma-ray burst (GRB) light curves is still lacking. Despite the diversity of GRBs, some general characteristics and correlations have been identified: spectral lag is one such characteristic. The spectral lag is the difference in time of arrival of high-energy pulses versus low-energy pulses. In our analysis, a positive spectral lag corresponds to an earlier arrival time for the higher energy photons. The observed spectral lag is a common feature in GRBs (Cheng et al. 1995; Norris et al. 1996; Band 1997). The study of spectral lag between energy bands, which combines temporal and spectral information, potentially can constrain GRB models (Lu et al. 2006; Shen et al. 2005; Qin et al. 2004; Schaefer 2004; Ioka & Nakamura 2001; Salmonson 2000).

Based on six GRBs with known redshifts, Norris et al. (2000) found an anti-correlation between the spectral lag and the isotropic peak luminosity. Further evidence for this correlation was provided by Norris (2002), Gehrels et al. (2006), Schaefer (2007), Stamatikos et al. (2008a), and Hakkila et al. (2008). Others have used this relation as a redshift indicator (Murakami et al. 2003; Band et al. 2004) and as a cosmological tool (Bloom et al. 2003; Schaefer 2007; Liang et al. 2008; Mosquera Cuesta et al. 2008).

Hakkila et al. (2008) have used a pulse-profile fitting technique (a four-parameter pulse function introduced by Norris et al. 2005) to show that the correlation is between lags of the pulses and the luminosity of the pulses seen in GRBs. However, the method is limited because it applies only to very bright bursts where pulses are clearly identifiable and described by the assumed pulse profile.

Many authors have tried to explain the physical cause of the lag–luminosity relation and a number of models have been proposed. Salmonson (2000) argues that the anti-correlation is due to the variations in the line-of-sight velocity of various GRBs. Ioka & Nakamura (2001) suggest that the relation is a result of variations of the off-axis angle when viewing a narrow jet. Schaefer (2004) invokes a rapid radiation cooling effect to explain the correlation. This effect tends to produce short spectral lags for highly luminous GRBs.

Regardless of its physical origin, the spectral lag is an important measurement for GRB science because of its usefulness in differentiating long and short GRBs (Kouveliotou et al. 1993): long bursts give large lags and short bursts give relatively small lags (Norris 1995; Norris & Bonnell 2006). Even though a few exceptions to this classification scheme have been found, such as GRB 060614 (Gehrels et al. 2006), the GRB community still continues to use the spectral lag as one of the classification criteria. Note that more elaborate classification schemes based on multiple observational parameters, such as the host galaxy property, has also been proposed (Donaghy et al. 2006; Zhang et al. 2009).

Moreover, based on the analysis of GRB 080319B, Stamatikos et al. (2009) show that there is a possible correlation between the prompt optical emission and the evolution of spectral lag with time.

Most of the previous work on spectral lags has been based on observations with the Burst and Transient Source Experiment (BATSE) on the Compton Gamma Ray Observatory (Tsutsui et al. 2008; Hakkila et al. 2008, 2007; Chen et al. 2005; Band et al. 2004; Salmonson & Galama 2002; Norris 2002; Band

[7] Center for Cosmology and Astro-Particle Physics (CCAPP) Fellow.

1997). The launch of the *Swift* satellite (Gehrels et al. 2004) ushered in a new era of GRB research. In this paper, we present a detailed study of spectral lags using a subset of *Swift* Burst Alert Telescope (BAT) data.

The structure of the paper is as follows. In Section 2, we discuss our methodology with a case study featuring GRB 060206. In Section 3, we present our results for a sample of 31 *Swift* BAT long bursts and investigate the lag–luminosity relation for various channel combinations. Finally, in Section 4, we discuss some implications of our results. Throughout this paper, the quoted uncertainties are at the 68% confidence level.

2. METHODOLOGY

2.1. Light-curve Extraction

Swift BAT is a highly sensitive instrument, which utilizes a coded aperture mask to localize bursts (Barthelmy et al. 2005). The basic imaging scheme is that a gamma-ray source illuminates the coded aperture mask and casts a shadow onto a position sensitive detector. Each position in the sky will produce a unique shadow pattern in the detector plane. Hence by comparing the observed shadow with precalculated shadow patterns for all possible points in the sky it is possible to find the actual position of the source that created the given shadow pattern. However, in practice each detector can be illuminated by many points on the sky whereas each point on the sky can illuminate many detectors. To disentangle each point in the sky, special software designed by the *Swift* BAT team is used.

In order to generate light curves, a process called mask weighting is utilized. The mask weighting assigns a ray-traced shadow value for each individual event, which then enables the user to calculate light curves or spectra. We used the `batmaskwtevt` and `batbinevt` tasks in FTOOLS to generate mask weighted, background-subtracted light curves for our analysis. Resulting light curves and their uncertainties are calculated by propagation of errors from raw counts (subject to Poissonian noise).

2.2. The Cross-correlation Function and Spectral Lag

There are at least three well-known ways of extracting spectral lags: (1) pulse peak-fit method (Norris et al. 2005; Hakkila et al. 2008), (2) Fourier analysis method (Li et al. 2004), and (3) cross-correlation function (CCF) analysis method (Cheng et al. 1995; Band 1997). The pulse peak-fit method gives a simple straight forward way for extracting lags. It does however assume a certain pulse function for the pulses in the light curve and may also be limited to very bright bursts. It is not immediately clear how this method would fare in cases where the light curves are sufficiently complex, i.e., not dominated by a prominent pulse. For transient events such as GRBs using the Fourier analysis technique also has its difficulties (Li et al. 2004). Since GRB light curves do not exhibit obvious periodicities, Fourier transforms typically yield a large number of coefficients to describe their temporal structure. These coefficients, in turn, produce a spectral lag value for each corresponding frequency component, i.e., a spectrum of lags is generated. The generated spectra exhibit a variety of shapes depending on the complexity of the light curve (Li et al. 2004) thus making the extraction of an intrinsic lag questionable. Hence, in this work, we develop a method to calculate the time-averaged spectral lag and its uncertainty via a modification of the CCF method.

The use of the Pearson CCF is a standard method of estimating the degree to which two series are correlated. For two counting series x_i and y_i where $i = 0, 1, 2, \ldots (N-1)$, the CCF with a delay d is defined as

$$\mathrm{CCF}_{\mathrm{Std}}(d, x, y) = \frac{\sum_{i=1}^{N-d}(x_i - \bar{x})(y_{i+d} - \bar{y})}{\sqrt{\sum_i (x_i - \bar{x})^2}\sqrt{\sum_i (y_i - \bar{y})^2}}. \quad (1)$$

Here $\bar{x}$ and $\bar{y}$ are average counts of the two series x and y, respectively. The denominator in the expression above serves to normalize the correlation coefficient such that $-1 \leqslant \mathrm{CCF}_{\mathrm{Std}}(d, x, y) \leqslant 1$, the bounds indicating maximum correlation and zero indicating no correlation. A high negative correlation indicates a high correlation but of the inverse of one of the series. Note that the time delay (τ) is given by $\tau = d \times$ time bin size.

However, Band (1997) proposed that for transient events such as GRBs, non-mean subtracted definition given below is more suitable for the time-averaged lag,

$$\mathrm{CCF}_{\mathrm{Band}}(d, x, y) = \frac{\sum_{i=\max(1,1-d)}^{\min(N,N-d)} x_i\, y_{i+d}}{\sqrt{\sum_i x_i^2 \sum_i y_i^2}}. \quad (2)$$

We have tested both definitions of the CCF using synthetic light curves with artificially introduced spectral lags. Our tests showed that the $\mathrm{CCF}_{\mathrm{Band}}$ consistently recovered the introduced lag, while $\mathrm{CCF}_{\mathrm{Std}}$ sometimes failed (possible reasons for this failure are noted in Band 1997). Hence, in our analysis we used the $\mathrm{CCF}_{\mathrm{Band}}$ definition and from this point onward in the paper we refer to it simply as the CCF.

For a given pair of real light curves, we determine the CCF using Equation (2). At this stage the resulting CCF values do not have any uncertainties associated with them. In order to determine these uncertainties, we use a Monte Carlo simulation. Here we make 1000 Monte Carlo realizations of the real light curve-pair based on their error bars as shown below:

$$\mathrm{LC}_{\mathrm{bin}}^{\mathrm{simulated}} = \mathrm{LC}_{\mathrm{bin}}^{\mathrm{real}} + \xi \times \mathrm{LC}_{\mathrm{bin}}^{\mathrm{real\,error}}, \quad (3)$$

where ξ is a random number generated from a Gaussian distribution with the mean equal to zero and the standard deviation equal to one. For each simulated light curve-pair we calculate the CCF value for a series of time delays. This results in a 1000 CCF values per time-delay bin. The standard deviation of these values per time-delay bin is then assigned as the uncertainty in the original CCF values obtained from the real light curves.

2.3. Extracting Spectral Lags

We realize that there may be a number of ways to define the spectral lag, but in this work, we define it as the time delay corresponding to the global maximum of the CCF. To locate this global maximum, we fit a Gaussian curve to the CCF. The uncertainties in the CCF are obtained using a Monte Carlo procedure discussed in Section 2.2. In essence, our fitting procedure locates the centroid of the CCF and is thus relatively insensitive to spurious spikes in the CCF. We tested and verified the robustness of this procedure by performing a number of simulations in which artificial lags were first introduced into the light curves and then successfully recovered. In addition, our tests with these artificial light curves show that the CCF can become asymmetric (around its global maximum) if the shape of one of the light curves is significantly different from the other. This energy-dependent feature potentially requires a

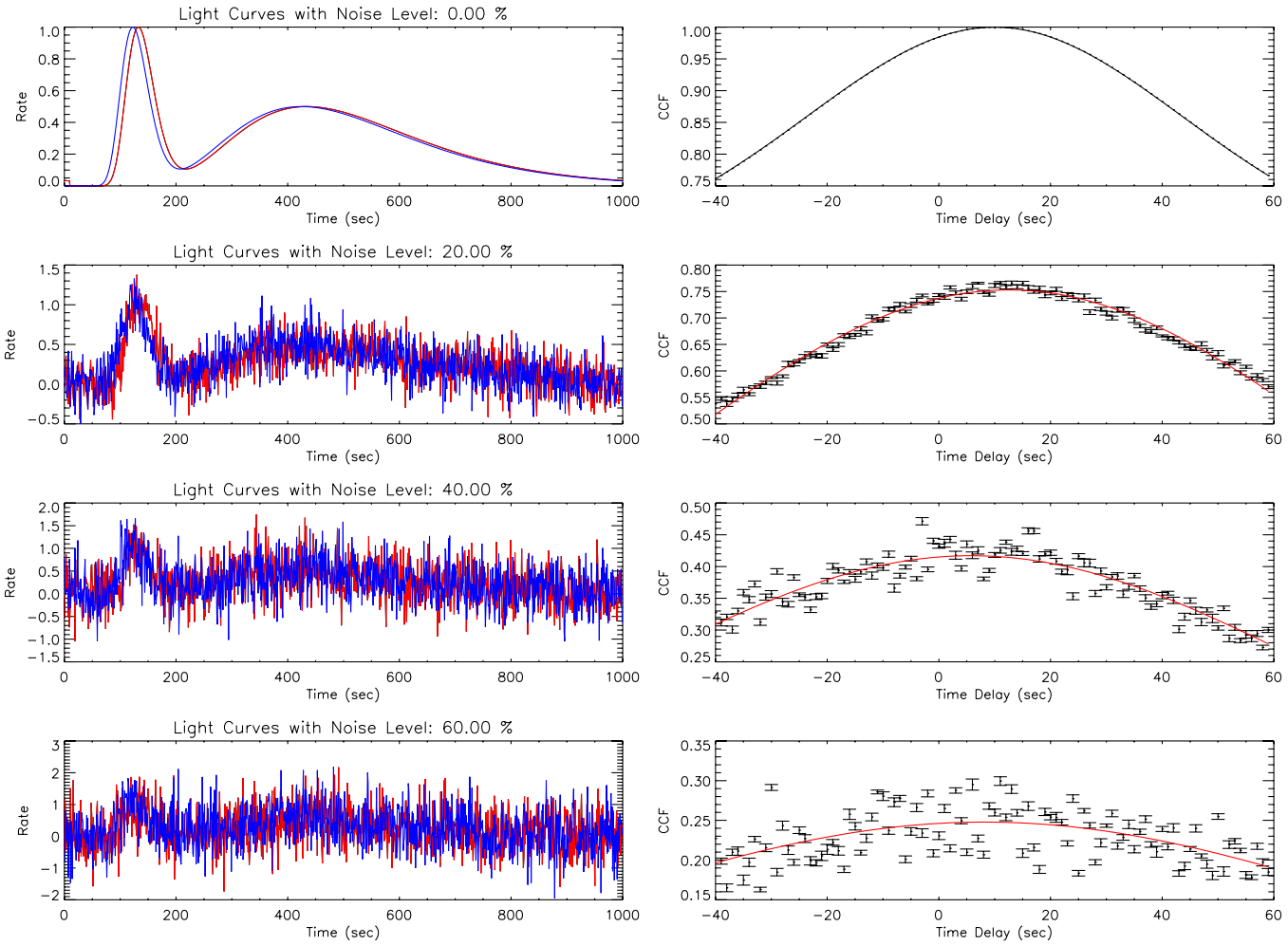

Figure 1. Effect of noise on the CCF. Panels on the left show two synthetic light curves, in which a 10 s artificial lag is added. From top to bottom the noise level is increased as 0%, 20%, 40%, and 60%, respectively. The corresponding CCF vs. time delay plots are shown in the right panels along with Gaussian fits.
(A color version of this figure is available in the online journal.)

more complex fitting function than a Gaussian or a quadratic to fit the CCF over the entire range. Instead of resorting to a more complex fitting function we were able to recover the (known) lags by fitting the CCFs (with a Gaussian) over limited but asymmetric ranges.

2.3.1. Time Bin Selection

For *Swift* GRBs the minimum time binning is 0.1 ms but one can arbitrarily increase this all the way up to the duration of the burst. It is important to understand the effect of time binning on the extracted spectral lags. Presumably, by changing the time binning of the light curve one is affecting the signal-to-noise ratio. By employing increasingly coarser binning one is averaging over the high frequency components of the light curve. Clearly, one has to be careful not to use overly large time bin sizes otherwise one risks losing the sought-after information from the light curve.

In order to understand the effect of time binning more fully, we did a number of simulations utilizing peak normalized synthetic light curves (composed of FRED[8]-like pulse shapes with Gaussian distributed noise) in which artificial lags were introduced. We incrementally increased the noise level and studied its effect on the maximum correlation value in the CCF versus time delay (CCFMax) plot. In Figure 1, we display the synthetic light curves with several noise levels (0%, 20%, 40%, and 60% respectively) as well as the calculated CCF with typical Gaussian fits. As expected, the CCFMax value (see the right panel of Figure 1) decreases gradually as the noise level increases. We also note that the scatter in the CCF increases considerably with the noise level. The global maximum in the CCF is clearly visible at the 40% noise level and a good fit is obtained with a Gaussian. However, this is not the case for the 60% noise-level curve, in which the scatter is quite significant, and the CCF global maximum is barely visible leading to a poor fit.

In Figure 2, we show the behavior of the CCFMax value and the extracted spectral lag as a function of the noise level. We first note that the CCFMax value smoothly tracks the signal-to-noise level in the light curves (see the upper panel of Figure 2). Second, we note that the extracted lag value agrees well with the artificially introduced lag of 10 s up to a noise level of about 40%. We further note that the scatter in the extracted lag value increases as the noise contribution increases beyond 40%. Although it is not immediately obvious from this figure, CCF values above a noise level of 40% show large scatter (see bottom right panel of Figure 1), thus making the extracted lag value uncertain. This is directly reflected by the increasing error

[8] Fast rise exponential decay.

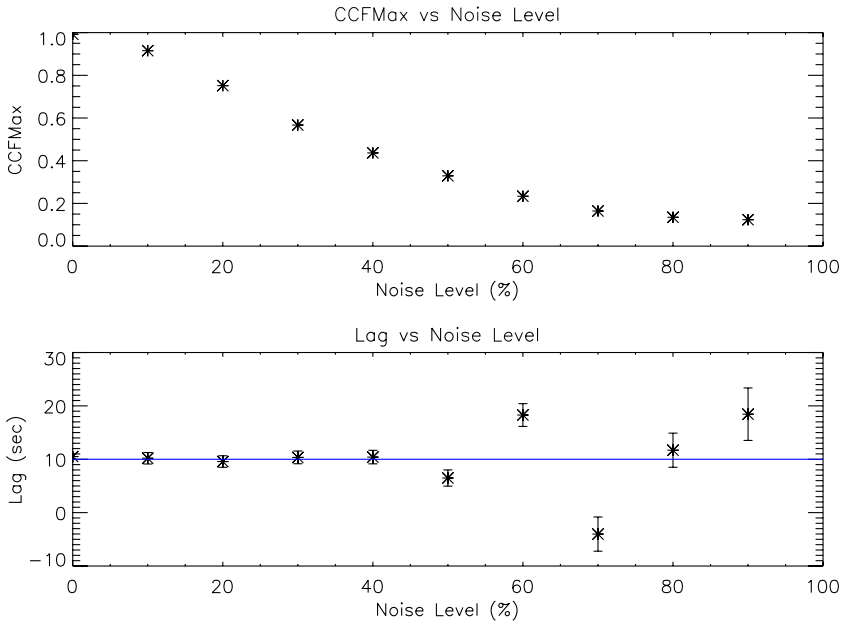

Figure 2. Effect of noise on the maximum correlation of the CCF (CCFMax) and the extracted spectral lag. The horizontal line (blue) in the bottom panel indicates the 10 s artificial lag.

(A color version of this figure is available in the online journal.)

bars in the extracted value. These simulations were repeated for number of time lags and in all cases similar results were obtained, in particular, the behavior of the CCFMax as a function of the noise level was confirmed. Based on the results of these simulations, we chose a CCFMax $\sim$ 0.5, corresponding to a noise level of about 40%, as our guide for picking the appropriate time binning.

Procedurally, we start with a time bin size of 1024 ms and decrease the time binning by powers of 2 until the CCFMax becomes $\sim$0.5 and use that time bin size as the preferred time binning for the lag extraction. By using this procedure we are able to arrive at a reasonable bin size that preserves the fine structure in the light curve and at the same time keeps the contribution of the noise component at a manageable level.

2.3.2. Uncertainty in Spectral Lags

We have studied three methods to determine the uncertainty in the extracted spectral lags. The first method is to use the uncertainty that is obtained by fitting the CCF with a Gaussian curve. The second method is an adaptation of Equation (4) used in Gaskell & Peterson (1987)

$$\sigma_{\rm lag} = \frac{0.75\, W_{\rm HWHM}}{1 + h\sqrt{n-2}}. \quad (4)$$

Here $W_{\rm HWHM}$ is the half-width half-maximum of the fitted Gaussian, h is the maximum height of the Gaussian, and n is the number of bins in the CCF versus time delay plot. This method utilizes more information about the fit and the CCF such as the width, height, and number of bins to estimate the uncertainty. The third method utilizes a Monte Carlo simulation. We found that the first method gives systematically smaller uncertainty in the lag by a factor of 2 or more relative to the other two methods. The second and third methods give comparable values. We adopted the most conservative of the three methods (i.e., the one based on the Monte Carlo simulation) to determine the uncertainties in the lag.

2.3.3. Lag Extraction: Case Study

To illustrate the lag extraction procedure more clearly, we present a case study using GRB 060206. The light-curve segment is selected by scanning both forward and backward directions from the peak location until the count rate drops to less than 5% of the peak count rate (using 15–200 keV light curve). This selection method is chosen to include the most intense segment of the burst and to capture any additional overlapping pulses near the main structure. Presumably, these pulses also contribute to the overall spectral lag. In the case of GRB 060206, this corresponds to a light-curve segment starting 1.29 s prior to the trigger and 8.18 s after the trigger (see Figure 3). Next we calculate the CCF and plot it as a function of time delay as shown Figure 4. Error bars on the CCF points were obtained via a Monte Carlo simulation of 1000 realizations of the original light curves (see Section 2.2). As noted earlier, we start with time bin size of 1024 ms and decrease the time binning by powers of 2 until the CCFMax becomes $\sim$0.5 for a given channel combination, in this case BAT standard channel 2 (25–50 keV) and 3 (50–100 keV). For GRB 060206 channels 2 and 3, the time bin size corresponds to 8 ms. The global maximum of the CCF versus time delay plot corresponds to the spectral lag and its value is obtained by fitting a Gaussian curve. We choose a range of the time delay (in this case from -1.5 s to 1.5 s) manually to identify the global maximum. In order to obtain the uncertainty in the spectral lag, we employ another Monte Carlo simulation, in which we create 1000 additional realizations of the input light curves as described in Section 2.2, and repeat the previously described process for the simulated light curves. A histogram of the resulting (1000) spectral lag values is shown in Figure 5 for GRB 060206. The standard deviation of these values is the uncertainty in the spectral lag.

2.4. Isotropic Peak Luminosity

To compare observations with different instruments we need to calculate flux over some fixed energy band. In order to do this

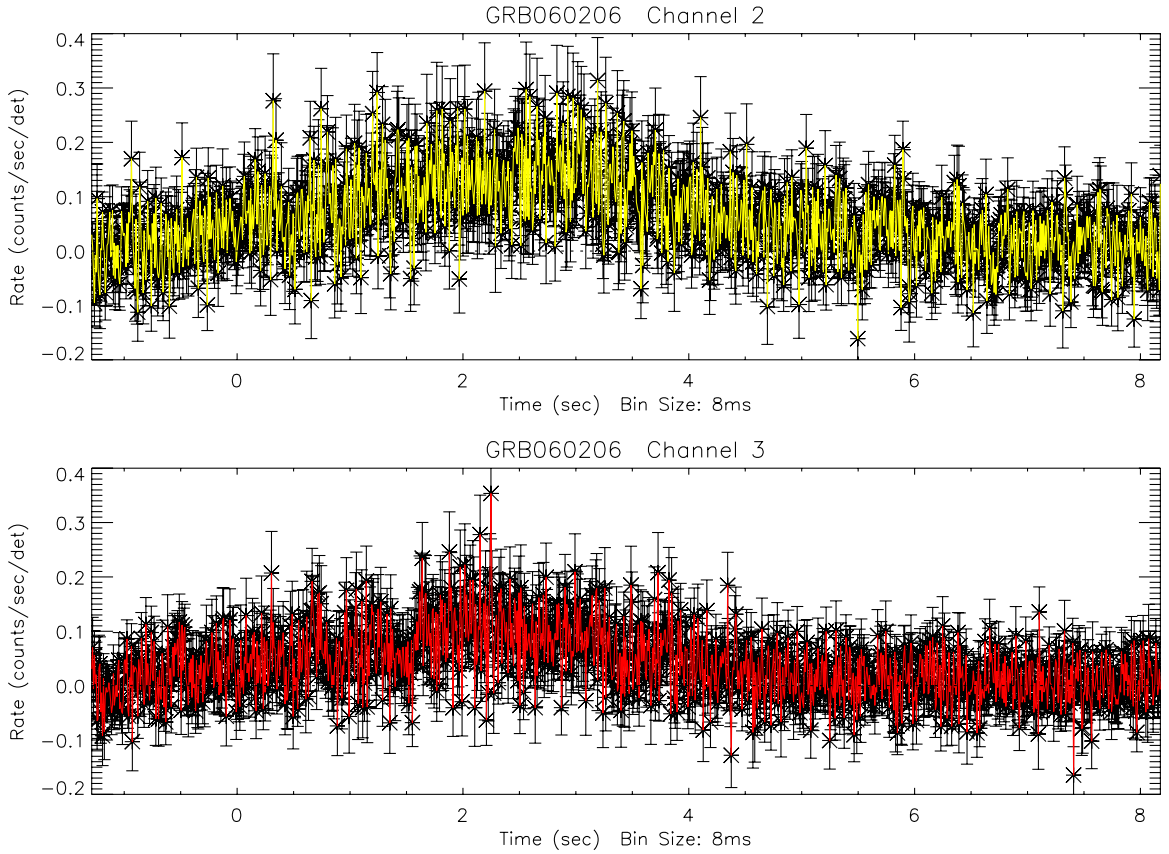

Figure 3. *Swift*/BAT prompt gamma-ray (8 ms time bin) light curves for GRB 060206 with canonical energy channels 2 (25–50 keV) and 3 (50–100 keV).
(A color version of this figure is available in the online journal.)

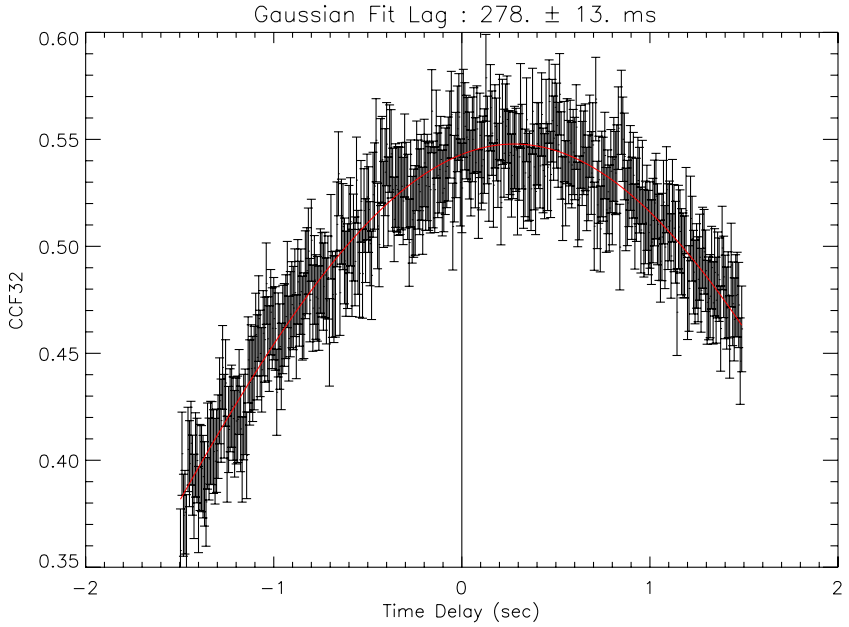

Figure 4. CCF as a function of time delay for the two light curves in Figure 3. The time delay corresponding to the peak of the Gaussian fit is the spectral lag of the burst, which is 278 ± 13 ms. The uncertainty quoted here is from the fit, which tends to be factor of 2 or more less than the value obtained by the Monte Carlo simulation shown in Figure 5.

(A color version of this figure is available in the online journal.)

we need to know the best-fit spectral function to the observed spectrum and its spectral parameters. Often, GRB spectra can be well fitted with the Band function (Band et al. 1993), an empirical spectral model defined as follows:

$$N = \begin{cases} A\left(\frac{E}{100\,\mathrm{keV}}\right)^{\alpha} e^{-(2+\alpha)E/E_{\mathrm{p}}}, & E \leqslant \left(\frac{\alpha-\beta}{2+\alpha}\right) E_{\mathrm{p}} \\ A\left(\frac{E}{100\,\mathrm{keV}}\right)^{\beta} \left[\frac{(\alpha-\beta)E_{\mathrm{p}}}{(2+\alpha)100\,\mathrm{keV}}\right]^{\alpha-\beta} e^{(\beta-\alpha)}, & \text{otherwise.} \end{cases}$$

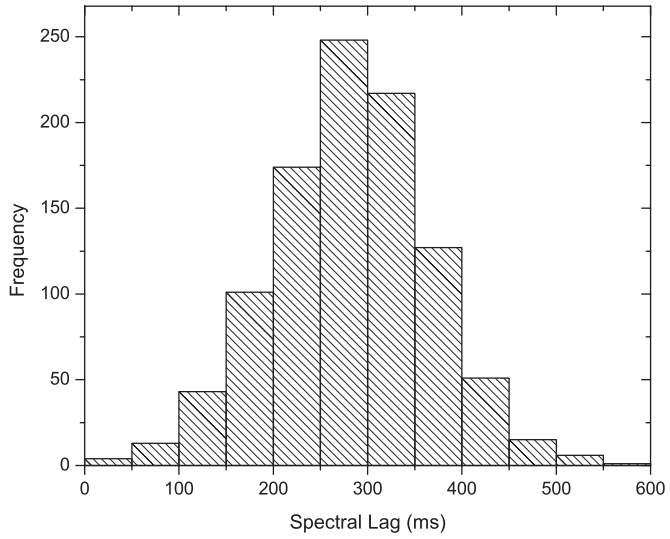

Figure 5. Histogram of 1000 simulated spectral lag values. We take the standard deviation of the distribution of simulated spectral lag values as the uncertainty of the fitted spectral lag value which was found in Figure 4. The final spectral lag value is 278 ± 74 ms.

There are four model parameters in the Band function; the amplitude (A), the low-energy spectral index (α), the high-energy spectral index (β), and the peak of νF_ν spectrum ($E_{\rm p}$).

If the GRB spectrum is well described by the Band function, then the values of α, β, E_p and the observed peak flux, $f_{\rm obs}$, in a given energy band ($E_{\rm min}$ and $E_{\rm max}$) are often reported. We can calculate the normalization A with

$$A = \frac{f_{\rm obs}}{\int_{E_{\rm min}}^{E_{\rm max}} N'(E)\,dE}, \tag{5}$$

where $f_{\rm obs}$ is given in photons cm^{-2} s^{-1} and $N' = N/A$.

The observed peak flux for the source-frame energy range $E_1 = 1.0$ keV to $E_2 = 10{,}000$ keV is

$$f_{\rm obs}^{\rm new} = \int_{E_1/(1+z)}^{E_2/(1+z)} N(E) E\,dE. \tag{6}$$

The isotropic peak luminosity is

$$L_{\rm iso} = 4\pi d_L^2\, f_{\rm obs}^{\rm new}, \tag{7}$$

where d_L is the luminosity distance given by

$$d_L = \frac{(1+z)c}{H_0} \int_0^z \frac{dz'}{\sqrt{\Omega_M (1+z')^3 + \Omega_L}}. \tag{8}$$

For the current universe we have assumed, $\Omega_M = 0.27$, $\Omega_L = 0.73$, and the Hubble constant H_0 is $70\,({\rm km\,s^{-1}})$ Mpc^{-1} $= 2.268 \times 10^{-18}$ s^{-1} (Komatsu et al. 2009).

To determine the uncertainty in $L_{\rm iso}$, we employ a Monte Carlo simulation. We simulate spectral parameters α, β, $E_{\rm p}$ and flux assuming their reported value as sample mean and reported uncertainty as sample standard deviation, then calculate $L_{\rm iso}$, for 1000 variations in these parameters. If a parameter has uneven uncertainty values then each side around the parameter is simulated with different uncertainty values as standard deviation. Then we take the 16th and the 84th ranked values (1σ uncertainty) as the lower limit and the upper limit of $L_{\rm iso}$, respectively.

3. RESULTS

We selected a sample of long GRBs ($T90 > 2$ s, excluding short bursts with extended emission), detected by *Swift* BAT from 2004 December 19 to 2009 July 19, for which spectroscopically confirmed redshifts were available. Out of this initial sample (102), a subset of 41 GRBs were selected with peak rate > 0.3 counts s^{-1} det^{-1} (15–200 keV, 256 ms time resolution). Finally, we selected 31 GRBs for which a clear global maximum can be seen in the CCF versus time delay plots with maximum correlation of at least 0.5 (with 256 ms time binning) for all channel combinations. The spectral parameters of the final sample are given in Table 1. We note that our final sample contains bursts with redshifts ranging from 0.346 (GRB 061021) to 5.464 (GRB 060927) and the average redshift of the sample is ~2.0.

Out of our sample, 18 bursts have all Band spectral parameters measured and comprise our "Gold" sample. The remaining 13 bursts are further divided into "Silver" and "Bronze" samples. In the "Silver" sample, ten bursts have $E_{\rm p}$ determined by fitting a cutoff power-law[9] (CPL) to spectra and for GRB 060418, $E_{\rm p}$ is reported without uncertainty, so we assumed a value of 10%. These ten bursts do not have the high-energy spectral index, β, measured, so we used the mean value of the BATSE β distribution, which is -2.36 ± 0.31 (Kaneko et al. 2006; Sakamoto et al. 2009). The "Bronze" sample (consisting of 3 bursts) does not have a measured $E_{\rm p}$. We have estimated it using the power-law (PL) index (Γ) of a simple PL fit as described in Sakamoto et al. (2009). For these three bursts, the low-energy spectral index, α, and the high-energy spectral index, β, were not known, so we used the mean value of the BATSE α and β distribution, which is -0.87 ± 0.33 and -2.36 ± 0.31, respectively (Kaneko et al. 2006; Sakamoto et al. 2009). All estimated spectral parameters are given in square brackets in Table 1.

Using the spectral parameters and redshift information in Table 1 we have calculated the peak isotropic luminosities for all the bursts in our sample: these results are shown in Table 2. GRB 080430 has the lowest luminosity in the sample ($\sim 1.03 \times 10^{51}$ erg s^{-1}), and GRB 080607 has the highest luminosity ($\sim 7.19 \times 10^{53}$ erg s^{-1}). The sample spans roughly 3 orders of magnitude in luminosity.

We extracted the spectral lags for all combinations of the canonical BAT energy bands: channel 1 (15–25 keV), 2 (25–50 keV), 3 (50–100 keV), and 4 (100–200 keV). We took the upper-boundary of channel 4 to be 200 keV because we found that after the mask weighting the contribution to the light curve from energies greater than ~200 keV is negligible. The nomenclature is straightforward, i.e., the spectral lag between energy channels 4 and 1 is represented by Lag 41. As such, there are six channel combinations and the results for all six are shown in Table 3. The segment of the light curve used for the lag extraction ($T + X_{\rm S}$ and $T + X_{\rm E}$, where T is the trigger time), the time binning of the light curve, and the Gaussian curve fitting range of the CCF versus time delay plot (with start time, and end time denoted as LS and LE, respectively) are also given in Table 3.

We noticed, as did Wu & Fenimore (2000), that the lag extraction is sensitive to a number of parameters. Hence, in Table 3, we specify the band pass that we used to extract the lag, segment of the light curve used, temporal bin resolution, and the fitting range used in the CCF versus time delay plot. These additional parameters are reported in order to facilitate

[9] $dN/dE \sim E^\alpha \exp(-(2+\alpha)E/E_{\rm p})$

Table 1
GRB Redshift and Spectral Information

GRB	z	Peak Flux[a]	E_p[b]	α[c]	β[d]	Reference
GRB050401	2.899[1]	10.70 ± 0.58	119^{+16}_{-16}	$0.83^{+0.13}_{-0.13}$	$2.37^{+0.09}_{-0.09}$	Golenetskii et al. (2005b); Sakamoto et al. (2008)
GRB050603	2.821[2]	21.50 ± 0.67	349^{+18}_{-18}	$0.79^{+0.04}_{-0.04}$	$2.15^{+0.06}_{-0.06}$	Golenetskii et al. (2005a); Sakamoto et al. (2008)
GRB050922C	2.199[3]	7.26 ± 0.20	$[133^{+468}_{-39}]$	$[0.87^{+0.33}_{-0.33}]$	$[2.36^{+0.31}_{-0.31}]$	Sakamoto et al. (2008)
GRB051111	1.550[4]	2.66 ± 0.13	447^{+206}_{-175}	$1.22^{+0.09}_{-0.09}$	$2.10^{+0.27}_{-4.94}$	Krimm et al. (2009); Sakamoto et al. (2008)
GRB060206	4.056[5]	2.79 ± 0.11	75^{+12}_{-12}	$1.06^{+0.21}_{-0.21}$	$[2.36^{+0.31}_{-0.31}]$	Palmer et al. (2006); Sakamoto et al. (2008)
GRB060210	3.913[6]	2.72 ± 0.18	207^{+66}_{-47}	$1.18^{+0.11}_{-0.11}$	$[2.36^{+0.31}_{-0.31}]$	Krimm et al. (2009); Sakamoto et al. (2008)
GRB060418	1.490[7]	6.52 ± 0.22	230^{+23}_{-23}	$1.50^{+0.09}_{-0.09}$	$[2.36^{+0.31}_{-0.31}]$	Golenetskii et al. (2006d); Sakamoto et al. (2008)
GRB060904B	0.703[8]	2.44 ± 0.13	103^{+59}_{-26}	$0.61^{+0.42}_{-0.42}$	$1.78^{+0.16}_{-0.23}$	Krimm et al. (2009); Sakamoto et al. (2008)
GRB060908	1.884[9]	3.03 ± 0.16	124^{+48}_{-24}	$0.89^{+0.20}_{-0.20}$	$2.24^{+0.34}_{-4.85}$	Krimm et al. (2009); Sakamoto et al. (2008)
GRB060927	5.464[10]	2.70 ± 0.11	72^{+16}_{-7}	$0.90^{+0.25}_{-0.25}$	$[2.36^{+0.31}_{-0.31}]$	Sakamoto et al. (2008)
GRB061007	1.262[11]	14.60 ± 0.23	498^{+34}_{-30}	$0.53^{+0.06}_{-0.05}$	$2.61^{+0.16}_{-0.31}$	Golenetskii et al. (2006c); Sakamoto et al. (2008)
GRB061021	0.346[12]	6.11 ± 0.17	777^{+343}_{-148}	$1.22^{+0.08}_{-0.09}$	$[2.36^{+0.31}_{-0.31}]$	Golenetskii et al. (2006a); Sakamoto et al. (2008)
GRB061121	1.315[13]	21.10 ± 0.29	606^{+56}_{-45}	$1.32^{+0.02}_{-0.03}$	$[2.36^{+0.31}_{-0.31}]$	Golenetskii et al. (2006b); Sakamoto et al. (2008)
GRB070306	1.496[14]	4.07 ± 0.13	$[76^{+131}_{-52}]$	$[0.87^{+0.33}_{-0.33}]$	$[2.36^{+0.31}_{-0.31}]$	Sakamoto et al. (2008)
GRB071010B	0.947[15]	7.70 ± 0.19	52^{+6}_{-9}	$1.25^{+0.46}_{-0.31}$	$2.65^{+0.18}_{-0.31}$	Golenetskii et al. (2007b); Markwardt et al. (2007)
GRB071020	2.145[16]	8.40 ± 0.19	322^{+50}_{-33}	$0.65^{+0.17}_{-0.20}$	$[2.36^{+0.31}_{-0.31}]$	Golenetskii et al. (2007a); Holland et al. (2007)
GRB080319B	0.937[17]	24.80 ± 0.31	651^{+8}_{-9}	$0.82^{+0.01}_{-0.01}$	$3.87^{+0.28}_{-0.68}$	Golenetskii et al. (2008d); Racusin et al. (2008)
GRB080319C	1.949[18]	5.20 ± 0.19	307^{+88}_{-58}	$1.01^{+0.08}_{-0.08}$	$1.87^{+0.09}_{-0.39}$	Golenetskii et al. (2008a); Stamatikos et al. (2008b)
GRB080411	1.030[19]	43.20 ± 0.56	259^{+22}_{-17}	$1.51^{+0.02}_{-0.03}$	$[2.36^{+0.31}_{-0.31}]$	Golenetskii et al. (2008c); Sato et al. (2008)
GRB080413A	2.433[20]	5.60 ± 0.13	126^{+82}_{-26}	$1.15^{+0.18}_{-0.18}$	$2.12^{+0.21}_{-4.93}$	Krimm et al. (2009); Marshall et al. (2008)
GRB080413B	1.101[21]	18.70 ± 0.04	67^{+8}_{-5}	$1.24^{+0.16}_{-0.16}$	$2.77^{+0.14}_{-0.17}$	Krimm et al. (2009); Barthelmy et al. (2008)
GRB080430	0.767[22]	2.60 ± 0.13	$[67^{+85}_{-51}]$	$[0.87^{+0.33}_{-0.33}]$	$[2.36^{+0.31}_{-0.31}]$	Guidorzi et al. (2008)
GRB080603B	2.689[23]	3.50 ± 0.13	71^{+10}_{-10}	$1.21^{+0.19}_{-0.19}$	$[2.36^{+0.31}_{-0.31}]$	Mangano et al. (2008)
GRB080605	1.640[24]	19.90 ± 0.38	297^{+29}_{-25}	$0.87^{+0.08}_{-0.08}$	$2.58^{+0.19}_{-0.53}$	Golenetskii et al. (2008b); Sbarufatti et al. (2008)
GRB080607	3.036[25]	23.10 ± 0.69	348^{+17}_{-17}	$0.76^{+0.04}_{-0.04}$	$2.57^{+0.11}_{-0.16}$	Golenetskii et al. (2008e); Mangano et al. (2008)
GRB080721	2.591[26]	20.90 ± 1.13	485^{+42}_{-37}	$0.93^{+0.07}_{-0.05}$	$2.43^{+0.15}_{-0.26}$	Golenetskii et al. (2008f); Marshall et al. (2008)
GRB080916A	0.689[27]	2.70 ± 0.13	121^{+50}_{-16}	$0.95^{+0.16}_{-0.16}$	$2.15^{+0.17}_{-4.91}$	Krimm et al. (2009); Ziaeepour et al. (2008)
GRB081222	2.770[28]	7.70 ± 0.13	134^{+6}_{-6}	$0.55^{+0.04}_{-0.04}$	$2.10^{+0.04}_{-0.04}$	Bissaldi & McBreen (2008); Grupe et al. (2009)
GRB090424	0.544[29]	71.00 ± 1.25	177^{+2}_{-2}	$0.90^{+0.01}_{-0.01}$	$2.90^{+0.06}_{-0.06}$	Connaughton (2009); Cannizzo et al. (2009)
GRB090618	0.540[30]	38.80 ± 0.50	156^{+7}_{-7}	$1.26^{+0.04}_{-0.01}$	$2.50^{+0.09}_{-0.21}$	McBreen et al. (2009); Schady et al. (2009)
GRB090715B	3.000[31]	3.80 ± 0.13	178^{+21}_{-14}	$0.86^{+0.14}_{-0.13}$	$[2.36^{+0.31}_{-0.31}]$	Golenetskii et al. (2009); Vetere et al. (2009)

Notes. Note that uncertainties of parameters that are reported with 90% confidence level have been reduced to 1σ level for consistency.
[a] 1 s peak photon flux measured in photon $cm^{-2}\ s^{-1}$ in the energy range 15–150 keV.
[b] Peak energy is given in keV. Values in brackets indicate estimated values using the method described in Sakamoto et al. (2009).
[c] Values in brackets indicate estimated high-energy photon index, α, which is the mean value of the BATSE α distribution (Kaneko et al. 2006; Sakamoto et al. 2009).
[d] Values in brackets indicate estimated high-energy photon index, β, which is the mean value of the BATSE β distribution (Kaneko et al. 2006; Sakamoto et al. 2009).

References. (1) Watson et al. 2006; (2) Berger & Becker 2005; (3) Piranomonte et al. 2008; (4) Penprase et al. 2006; (5) Fynbo et al. 2009; (6) Fynbo et al. 2009; (7) Prochaska et al. 2006; (8) Fynbo et al. 2009; (9) Fynbo et al. 2009; (10) Fynbo et al. 2009; (11) Fynbo et al. 2009; (12) Fynbo et al. 2009; (13) Fynbo et al. 2009; (14) Jaunsen et al. 2008; (15) Cenko et al. 2007; (16) Jakobsson et al. 2007; (17) D'Elia et al. 2009; (18) Fynbo et al. 2009; (19) Fynbo et al. 2009; (20) Fynbo et al. 2009; (21) Fynbo et al. 2009; (22) Cucchiara & Fox 2008; (23) Fynbo et al. 2009; (24) Fynbo et al. 2009; (25) Prochaska et al. 2009; (26) Fynbo et al. 2009; (27) Fynbo et al. 2009; (28) Cucchiara et al. 2008; (29) Chornock et al. 2009; (30) Cenko et al. 2009; (31) Wiersema et al. 2009.

reproduction of the results and direct comparison with other extraction techniques.

Figures 6 through 11 show log–log plots of isotropic peak luminosity versus redshift corrected spectral lag for various energy channel combinations. Red circles represent bursts from the "Gold" sample, blue diamonds show bursts from the "Silver" sample and green triangles are bursts from the "Bronze" sample. The best-fit PL curve is also shown in these plots with a dashed line. Since there is a large scatter in these plots, to compensate, the uncertainties of the fit parameters are multiplied by a factor of $\sqrt{\chi^2/\mathrm{ndf}}$ (see Table 4).[10] The dotted lines indicate the estimated 1σ confidence level, which is obtained from the cumulative fraction of the residual distribution taken from 16% to 84%.

It is interesting to note that GRB 080603B exhibits five negative lags out of six possible combinations. While these negative lags are not shown in the plots, it is worth noting that negative lags are not necessarily unphysical (Ryde 2005). Moreover, in the few cases where the uncertainty is large, i.e., the extracted lags are consistent with zero, these points are not plotted either but are listed in Table 3. We recognize that the

[10] ndf is the number of degrees of freedom.

Table 2
GRB Redshift and Calculated Isotropic Peak Luminosity

GRB	Redshift	Peak Isotropic Luminosity[a]	GRB	Redshift	Peak Isotropic Luminosity[a]
GRB050401	2.899	$(1.38^{+0.16}_{-0.13}) \times 10^{53}$	GRB080319B	0.937	$(6.96^{+0.32}_{-0.14}) \times 10^{52}$
GRB050603	2.821	$(6.32^{+0.47}_{-0.34}) \times 10^{53}$	GRB080319C	1.949	$(6.04^{+8.04}_{-0.42}) \times 10^{52}$
GRB050922C	2.199	$(5.17^{+28.00}_{-0.01}) \times 10^{52}$	GRB080411	1.030	$(5.49^{+1.11}_{-0.34}) \times 10^{52}$
GRB051111	1.550	$(1.55^{+0.61}_{-0.33}) \times 10^{52}$	GRB080413A	2.433	$(5.38^{+4.69}_{-0.83}) \times 10^{52}$
GRB060206	4.056	$(6.28^{+2.50}_{-0.62}) \times 10^{52}$	GRB080413B	1.101	$(1.51^{+0.15}_{-0.06}) \times 10^{52}$
GRB060210	3.913	$(8.53^{+2.75}_{-0.92}) \times 10^{52}$	GRB080430	0.767	$(1.03^{+1.30}_{-0.07}) \times 10^{51}$
GRB060418	1.490	$(1.96^{+0.43}_{-0.13}) \times 10^{52}$	GRB080603B	2.689	$(2.99^{+1.25}_{-0.30}) \times 10^{52}$
GRB060904B	0.703	$(2.18^{+3.59}_{-0.32}) \times 10^{51}$	GRB080605	1.640	$(1.15^{+0.56}_{-0.09}) \times 10^{53}$
GRB060908	1.884	$(1.54^{+22.50}_{-0.22}) \times 10^{52}$	GRB080607	3.036	$(7.19^{+0.64}_{-0.41}) \times 10^{53}$
GRB060927	5.464	$(1.17^{+0.43}_{-0.10}) \times 10^{53}$	GRB080721	2.591	$(5.18^{+0.83}_{-0.47}) \times 10^{53}$
GRB061007	1.262	$(1.01^{+0.20}_{-0.08}) \times 10^{53}$	GRB080916A	0.689	$(1.30^{+19.90}_{-0.15}) \times 10^{51}$
GRB061021	0.346	$(1.30^{+0.60}_{-0.13}) \times 10^{51}$	GRB081222	2.770	$(1.26^{+0.07}_{-0.06}) \times 10^{53}$
GRB061121	1.315	$(7.89^{+1.02}_{-0.47}) \times 10^{52}$	GRB090424	0.544	$(1.62^{+0.05}_{-0.04}) \times 10^{52}$
GRB070306	1.496	$(8.67^{+13.50}_{-0.27}) \times 10^{51}$	GRB090618	0.540	$(8.47^{+1.17}_{-0.34}) \times 10^{51}$
GRB071010B	0.947	$(4.24^{+1.72}_{-0.33}) \times 10^{51}$	GRB090715B	3.000	$(6.79^{+2.42}_{-0.71}) \times 10^{52}$
GRB071020	2.145	$(1.27^{+0.64}_{-0.15}) \times 10^{53}$			

Note.
[a] Isotropic equivalent peak photon luminosity in erg s^{-1} between GRB rest frame energy range 1 and 10,000 keV as described in Section 2.

omission of these negative and zero lags is a potential source of bias.

As seen in Figures 6 through 11, our results support the existence of the lag–luminosity correlation originally proposed by Norris et al. (2000). Table 4 lists the correlation coefficients for all six channel combinations. The lag for channel combination 31 has the lowest correlation with $L_{\rm iso}$, where the correlation coefficient is −0.60 (with chance probability of $\sim 1.5 \times 10^{-3}$) and the lag for channel 43 has the highest correlation with coefficient of −0.77 (with chance probability of $\sim 3.0 \times 10^{-4}$). However, we note that there is considerable scatter in the plots. The results of our best-fit curves for each energy band combinations are also given in Table 4. The mean value of the PL indices that we get for various channel combinations is 1.4 ± 0.3. Our value is consistent with the 1.14 PL index Norris et al. (2000) reported using lags between BATSE energy bands 100–300 keV and 25–50 keV. Our results are also consistent with Stamatikos et al. (2008a) and Schaefer (2007) who reported values of 1.16 ± 0.21 and 1.01 ± 0.10 (assuming an uncertainty of 10%), respectively.

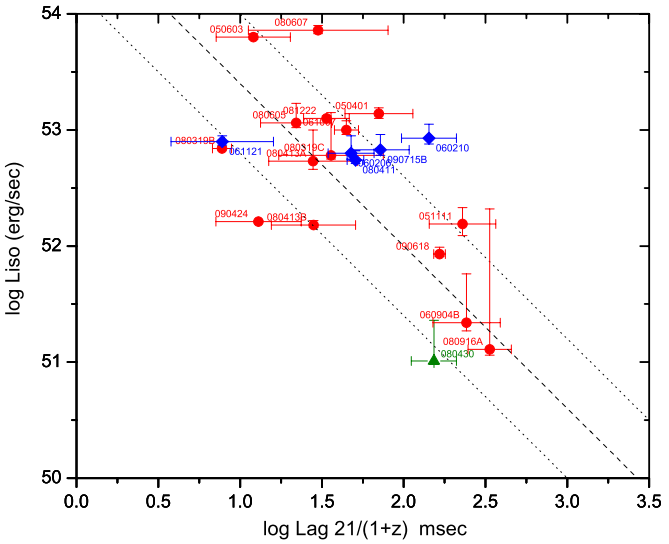

Figure 6. Isotropic luminosity as a function of spectral lag between BAT channels 2 (25–50 keV) and 1 (15–25 keV). The "Gold," "Silver," and "Bronze" samples are represented with red circles, blue diamonds, and green triangles, respectively.

(A color version of this figure is available in the online journal.)

4. DISCUSSION

Band (1997) showed that GRB spectra typically undergo hard-to-soft peak evolution, i.e., the burst peak moves to later times for lower energy bands. In our sample, we have six lag extractions for each burst. The perfect hard-to-soft peak evolution scenario is indicated by positive lag values for all channel combinations plus lag41 > lag42 > lag43 and lag31 > lag32. However, all bursts in our sample do not show this perfect behavior. Band (1997) used a scoring method to quantify the degree of hard-to-soft peak evolution. We used a more elaborate scoring method to assign a score to each GRB as follows: first, we increase the burst score by 1 if one of the six lag values is positive or decrease it by 1 if it is negative. Thus, a GRB can get a score ranging from −6 to +6 at this first step. Then, we compare the lag values of channel 4 as the base (lag43, lag42, and lag41). The score is increased by one if the burst meets one of the following conditions: lag41 > lag42, lag41 > lag43, or lag42 > lag43. We continue this procedure for channel 3 as the base also (lag31 > lag32). We decrease the score by 1 if it is otherwise. According to this scoring scheme a score of +10 corresponds to the perfect case that we mentioned earlier. A positive score indicates overall hard-to-soft peak evolution in the burst to some degree. A negative value indicates soft-to-hard peak evolution. Out of 31 bursts in our sample 19 bursts show perfect hard-to-soft peak evolution with a score of +10. About 97% of bursts in our sample have a score of greater than zero, which is consistent with the 90% value reported by Band (1997).

If one wants to use the lag–luminosity relation as a probe into the physics of GRBs (in the source rest frame), then a few corrections to the spectral lag are required: (1) correct

Table 3
Spectral Lag Values of Long Duration *Swift* BAT GRBs

GRB	Trigger ID	Lag *XX*	$T + X_S$ (s)	$T + X_E$ (s)	Bin Size (ms)	LS (s)	LE (s)	Lag Value (ms)
GRB050401	113120	Lag 21	23.03	29.43	32	−1.00	1.50	275 ± 131
		Lag 31	23.03	29.43	32	−1.00	2.00	504 ± 117
		Lag 41	23.03	29.43	64	−1.00	2.00	562 ± 140
		Lag 32	23.03	29.43	16	−1.00	1.00	136 ± 87
		Lag 42	23.03	29.43	64	−1.50	1.50	250 ± 112
		Lag 43	23.03	29.43	64	−2.00	2.00	106 ± 118
GRB050603	131560	Lag 21	−3.83	3.08	8	−0.40	0.40	46 ± 24
		Lag 31	−3.83	3.08	8	−0.40	0.40	59 ± 22
		Lag 41	−3.83	3.08	16	−0.40	0.40	86 ± 29
		Lag 32	−3.83	3.08	4	−0.20	0.20	4 ± 11
		Lag 42	−3.83	3.08	16	−0.40	0.40	34 ± 19
		Lag 43	−3.83	3.08	16	−0.50	0.50	20 ± 18
GRB050922C	156467	Lag 21	−2.70	2.94	8	−0.40	0.40	9 ± 35
		Lag 31	−2.70	2.94	8	−1.00	1.00	180 ± 50
		Lag 41	−2.70	2.94	16	−1.00	1.00	188 ± 78
		Lag 32	−2.70	2.94	4	−1.00	1.00	188 ± 39
		Lag 42	−2.70	2.94	16	−1.00	1.00	178 ± 70
		Lag 43	−2.70	2.94	16	−1.00	1.00	19 ± 72
GRB051111	163438	Lag 21	−6.96	28.62	32	−5.00	4.00	583 ± 273
		Lag 31	−6.96	28.62	32	−4.00	4.00	1383 ± 288
		Lag 41	−6.96	28.62	128	−4.00	8.00	2343 ± 397
		Lag 32	−6.96	28.62	16	−5.00	4.00	776 ± 200
		Lag 42	−6.96	28.62	64	−5.00	5.00	1486 ± 314
		Lag 43	−6.96	28.62	64	−5.00	5.00	866 ± 319
GRB060206	180455	Lag 21	−1.29	8.18	8	−1.50	1.50	241 ± 78
		Lag 31	−1.29	8.18	16	−1.00	2.00	517 ± 85
		Lag 41	−1.29	8.18	64	−1.50	2.00	331 ± 219
		Lag 32	−1.29	8.18	8	−1.50	1.50	278 ± 74
		Lag 42	−1.29	8.18	64	−1.50	1.50	82 ± 193
		Lag 43	−1.29	8.18	64	−2.00	2.00	−163 ± 189
GRB060210	180977	Lag 21	−3.37	5.08	64	−5.00	4.00	700 ± 270
		Lag 31	−3.37	5.08	64	−5.00	4.00	508 ± 254
		Lag 41	−3.37	5.08	256	−5.00	4.00	1038 ± 324
		Lag 32	−3.37	5.08	64	−4.00	4.00	−175 ± 174
		Lag 42	−3.37	5.08	128	−4.00	4.00	98 ± 225
		Lag 43	−3.37	5.08	256	−5.00	2.00	34 ± 195
GRB060418	205851	Lag 21	−7.66	33.04	16	−2.00	2.00	22 ± 62
		Lag 31	−7.66	33.04	32	−2.00	2.00	109 ± 62
		Lag 41	−7.66	33.04	128	−2.00	2.00	476 ± 196
		Lag 32	−7.66	33.04	16	−2.00	2.00	87 ± 50
		Lag 42	−7.66	33.04	64	−1.00	1.00	212 ± 100
		Lag 43	−7.66	33.04	64	−1.00	1.00	162 ± 101
GRB060904B	228006	Lag 21	−1.97	10.32	32	−2.00	2.00	412 ± 195
		Lag 31	−1.97	10.32	32	−2.00	2.00	560 ± 164
		Lag 41	−1.97	10.32	128	−3.00	3.00	602 ± 296
		Lag 32	−1.97	10.32	32	−2.00	2.00	247 ± 140
		Lag 42	−1.97	10.32	128	−2.50	3.00	175 ± 292
		Lag 43	−1.97	10.32	128	−3.00	3.00	32 ± 273
GRB060908	228581	Lag 21	−10.91	3.68	32	−2.00	2.00	118 ± 142
		Lag 31	−10.91	3.68	32	−2.00	2.00	346 ± 185
		Lag 41	−10.91	3.68	128	−4.00	4.00	367 ± 315
		Lag 32	−10.91	3.68	16	−2.00	2.00	124 ± 86
		Lag 42	−10.91	3.68	64	−2.00	2.00	233 ± 216
		Lag 43	−10.91	3.68	128	−4.00	4.00	134 ± 253
GRB060927	231362	Lag 21	−1.69	8.04	16	−0.60	0.60	9 ± 46
		Lag 31	−1.69	8.04	64	−1.00	1.00	74 ± 62
		Lag 41	−1.69	8.04	256	−1.50	1.50	200 ± 133
		Lag 32	−1.69	8.04	16	−1.00	1.00	103 ± 45
		Lag 42	−1.69	8.04	128	−1.20	1.50	229 ± 112
		Lag 43	−1.69	8.04	128	−1.20	1.50	126 ± 101
GRB061007	232683	Lag 21	23.86	65.08	2	−0.30	0.50	101 ± 17
		Lag 31	23.86	65.08	2	−0.30	0.50	154 ± 19
		Lag 41	23.86	65.08	4	−0.50	0.80	286 ± 28
		Lag 32	23.86	65.08	2	−0.20	0.20	30 ± 8
		Lag 42	23.86	65.08	2	−0.40	0.40	129 ± 17
		Lag 43	23.86	65.08	2	−0.30	0.40	82 ± 9

Table 3
(Continued)

GRB	Trigger ID	Lag *XX*	$T + X_S$ (s)	$T + X_E$ (s)	Bin Size (ms)	LS (s)	LE (s)	Lag Value (ms)
GRB061021	234905	Lag 21	−0.46	14.64	8	−1.00	1.00	−25 ± 52
		Lag 31	−0.46	14.64	8	−1.00	1.00	49 ± 51
		Lag 41	−0.46	14.64	32	−1.60	1.60	239 ± 85
		Lag 32	−0.46	14.64	8	−1.00	1.00	62 ± 42
		Lag 42	−0.46	14.64	32	−1.00	1.20	248 ± 78
		Lag 43	−0.46	14.64	32	−1.00	1.20	188 ± 79
GRB061121	239899	Lag 21	60.44	80.66	1	−0.20	0.20	18 ± 13
		Lag 31	60.44	80.66	1	−0.20	0.20	16 ± 12
		Lag 41	60.44	80.66	4	−0.40	0.40	26 ± 26
		Lag 32	60.44	80.66	1	−0.20	0.25	17 ± 7
		Lag 42	60.44	80.66	2	−0.20	0.25	28 ± 12
		Lag 43	60.44	80.66	2	−0.20	0.25	25 ± 11
GRB070306	263361	Lag 21	90.00	118.42	8	−2.00	2.00	88 ± 106
		Lag 31	90.00	118.42	16	−2.00	2.00	146 ± 100
		Lag 41	90.00	118.42	64	−4.00	6.00	1088 ± 391
		Lag 32	90.00	118.42	8	−2.00	2.00	114 ± 102
		Lag 42	90.00	118.42	64	−4.00	6.00	1098 ± 399
		Lag 43	90.00	118.42	64	−4.00	6.00	900 ± 408
GRB071010B	293795	Lag 21	−1.70	17.24	2	−1.00	1.00	−26 ± 48
		Lag 31	−1.70	17.24	4	−1.00	1.00	146 ± 52
		Lag 41	−1.70	17.24	32	−2.00	4.00	1024 ± 163
		Lag 32	−1.70	17.24	4	−1.00	1.00	185 ± 47
		Lag 42	−1.70	17.24	32	−2.00	4.00	1005 ± 157
		Lag 43	−1.70	17.24	32	−2.00	4.00	745 ± 161
GRB071020	294835	Lag 21	−3.22	1.14	2	−0.10	0.15	7 ± 7
		Lag 31	−3.22	1.14	2	−0.10	0.20	37 ± 12
		Lag 41	−3.22	1.14	8	−0.50	0.50	−50 ± 30
		Lag 32	−3.22	1.14	2	−0.10	0.25	47 ± 7
		Lag 42	−3.22	1.14	4	−0.10	0.30	69 ± 12
		Lag 43	−3.22	1.14	4	−0.20	0.30	28 ± 9
GRB080319B	306757	Lag 21	−2.85	57.57	2	−0.10	0.14	15 ± 2
		Lag 31	−2.85	57.57	2	−0.10	0.14	32 ± 3
		Lag 41	−2.85	57.57	2	−0.20	0.20	80 ± 17
		Lag 32	−2.85	57.57	2	−0.10	0.14	23 ± 2
		Lag 42	−2.85	57.57	2	−0.20	0.30	88 ± 8
		Lag 43	−2.85	57.57	2	−0.20	0.20	26 ± 5
GRB080319C	306778	Lag 21	−0.77	13.31	16	−1.00	1.00	106 ± 78
		Lag 31	−0.77	13.31	16	−2.00	2.00	216 ± 70
		Lag 41	−0.77	13.31	64	−2.00	2.00	89 ± 132
		Lag 32	−0.77	13.31	16	−1.00	1.00	134 ± 58
		Lag 42	−0.77	13.31	32	−1.00	1.00	−77 ± 95
		Lag 43	−0.77	13.31	32	−1.00	1.00	−119 ± 99
GRB080411	309010	Lag 21	38.46	48.45	2	−1.00	1.00	103 ± 12
		Lag 31	38.46	48.45	2	−1.00	1.00	220 ± 13
		Lag 41	38.46	48.45	2	−1.00	1.00	322 ± 27
		Lag 32	38.46	48.45	2	−1.00	1.00	122 ± 11
		Lag 42	38.46	48.45	2	−1.00	1.00	230 ± 26
		Lag 43	38.46	48.45	2	−1.00	1.00	112 ± 26
GRB080413A	309096	Lag 21	−0.42	9.05	8	−1.00	1.00	96 ± 60
		Lag 31	−0.42	9.05	8	−1.00	1.00	242 ± 65
		Lag 41	−0.42	9.05	64	−1.00	2.00	542 ± 125
		Lag 32	−0.42	9.05	8	−1.00	1.00	157 ± 43
		Lag 42	−0.42	9.05	32	−1.00	2.00	418 ± 111
		Lag 43	−0.42	9.05	32	−1.00	2.00	249 ± 108
GRB080413B	309111	Lag 21	−1.44	4.96	8	−1.00	1.00	59 ± 35
		Lag 31	−1.44	4.96	8	−1.00	1.00	144 ± 37
		Lag 41	−1.44	4.96	16	−1.00	1.00	353 ± 66
		Lag 32	−1.44	4.96	8	−1.00	1.00	82 ± 28
		Lag 42	−1.44	4.96	16	−1.00	1.00	276 ± 56
		Lag 43	−1.44	4.96	16	−1.00	1.00	188 ± 55
GRB080430	310613	Lag 21	−1.24	12.84	32	−2.00	2.00	270 ± 86
		Lag 31	−1.24	12.84	32	−2.00	2.00	391 ± 109
		Lag 41	−1.24	12.84	256	−4.00	4.00	730 ± 374
		Lag 32	−1.24	12.84	32	−2.00	2.00	83 ± 100
		Lag 42	−1.24	12.84	256	−4.00	4.00	540 ± 387
		Lag 43	−1.24	12.84	256	−4.00	4.00	388 ± 397

Table 3
(Continued)

GRB	Trigger ID	Lag *XX*	$T + X_S$ (s)	$T + X_E$ (s)	Bin Size (ms)	LS (s)	LE (s)	Lag Value (ms)
GRB080603B	313087	Lag 21	−0.54	5.10	16	−1.00	1.00	−222 ± 61
		Lag 31	−0.54	5.10	16	−1.00	1.00	−197 ± 67
		Lag 41	−0.54	5.10	32	−1.00	1.00	−427 ± 163
		Lag 32	−0.54	5.10	16	−1.00	1.00	50 ± 41
		Lag 42	−0.54	5.10	32	−1.00	0.50	−103 ± 71
		Lag 43	−0.54	5.10	32	−1.00	0.50	−172 ± 56
GRB080605	313299	Lag 21	−5.46	15.53	4	−1.00	1.00	58 ± 29
		Lag 31	−5.46	15.53	4	−1.00	1.00	98 ± 33
		Lag 41	−5.46	15.53	16	−0.50	1.20	196 ± 39
		Lag 32	−5.46	15.53	2	−0.30	0.40	73 ± 11
		Lag 42	−5.46	15.53	8	−0.30	0.40	96 ± 17
		Lag 43	−5.46	15.53	8	−0.30	0.40	39 ± 12
GRB080607	313417	Lag 21	−6.13	12.05	8	−0.40	0.40	121 ± 119
		Lag 31	−6.13	12.05	8	−0.40	0.60	163 ± 39
		Lag 41	−6.13	12.05	16	−0.40	0.60	194 ± 43
		Lag 32	−6.13	12.05	8	−0.40	0.40	19 ± 17
		Lag 42	−6.13	12.05	8	−0.40	0.40	64 ± 23
		Lag 43	−6.13	12.05	8	−0.40	0.40	25 ± 18
GRB080721	317508	Lag 21	−3.39	8.64	64	−2.00	2.00	99 ± 149
		Lag 31	−3.39	8.64	64	−2.00	2.00	122 ± 138
		Lag 41	−3.39	8.64	128	−2.00	2.00	341 ± 182
		Lag 32	−3.39	8.64	16	−0.80	0.80	16 ± 58
		Lag 42	−3.39	8.64	32	−0.80	0.80	256 ± 308
		Lag 43	−3.39	8.64	32	−0.80	0.80	167 ± 69
GRB080916A	324895	Lag 21	−2.66	39.58	16	−2.00	3.00	566 ± 172
		Lag 31	−2.66	39.58	32	−2.00	4.00	1468 ± 202
		Lag 41	−2.66	39.58	256	−4.00	6.00	2879 ± 271
		Lag 32	−2.66	39.58	32	−4.00	4.00	821 ± 100
		Lag 42	−2.66	39.58	128	−2.00	6.00	1900 ± 165
		Lag 43	−2.66	39.58	64	−2.00	4.00	842 ± 143
GRB081222	337914	Lag 21	−0.80	15.58	2	−0.80	1.20	127 ± 41
		Lag 31	−0.80	15.58	2	−0.80	1.00	262 ± 47
		Lag 41	−0.80	15.58	16	−2.00	3.00	610 ± 111
		Lag 32	−0.80	15.58	2	−0.80	0.80	113 ± 30
		Lag 42	−0.80	15.58	8	−1.80	2.80	444 ± 107
		Lag 43	−0.80	15.58	8	−1.80	2.80	197 ± 110
GRB090424	350311	Lag 21	−0.94	4.95	1	−0.10	0.25	20 ± 12
		Lag 31	−0.94	4.95	2	−0.10	0.25	29 ± 13
		Lag 41	−0.94	4.95	4	−0.10	0.25	39 ± 15
		Lag 32	−0.94	4.95	1	−0.10	0.25	23 ± 9
		Lag 42	−0.94	4.95	4	−0.10	0.25	27 ± 13
		Lag 43	−0.94	4.95	4	−0.20	0.30	17 ± 9
GRB090618	355083	Lag 21	46.01	135.35	4	−1.00	1.00	255 ± 21
		Lag 31	46.01	135.35	4	−1.00	1.00	447 ± 26
		Lag 41	46.01	135.35	4	−1.00	2.00	894 ± 43
		Lag 32	46.01	135.35	4	−1.00	1.00	173 ± 18
		Lag 42	46.01	135.35	4	−1.00	1.50	483 ± 34
		Lag 43	46.01	135.35	4	−1.00	1.50	283 ± 34
GRB090715B	357512	Lag 21	−4.80	21.06	16	−2.50	2.50	288 ± 117
		Lag 31	−4.80	21.06	16	−2.50	2.50	732 ± 127
		Lag 41	−4.80	21.06	64	−2.50	3.00	1080 ± 224
		Lag 32	−4.80	21.06	8	−2.50	2.50	470 ± 100
		Lag 42	−4.80	21.06	32	−2.50	2.50	928 ± 229
		Lag 43	−4.80	21.06	32	−2.50	2.50	375 ± 215

Table 4
Correlation Coefficients and Fit Parameters

Channels	Correlation	Best Fit	χ^2/ndf
Channel 21	−0.63	$\log L_{iso} = (54.8 \pm 0.2) - (1.4 \pm 0.1) \log Lag21(1+z)^{-1}$	189.4/19
Channel 32	−0.66	$\log L_{iso} = (54.5 \pm 0.2) - (1.2 \pm 0.1) \log Lag32(1+z)^{-1}$	216/25
Channel 31	−0.60	$\log L_{iso} = (55.5 \pm 0.2) - (1.5 \pm 0.1) \log Lag31(1+z)^{-1}$	410.8/26
Channel 43	−0.77	$\log L_{iso} = (55.0 \pm 0.3) - (1.4 \pm 0.1) \log Lag43(1+z)^{-1}$	109/20
Channel 42	−0.75	$\log L_{iso} = (55.4 \pm 0.1) - (1.4 \pm 0.1) \log Lag42(1+z)^{-1}$	178.8/23
Channel 41	−0.67	$\log L_{iso} = (56.7 \pm 0.3) - (1.8 \pm 0.1) \log Lag41(1+z)^{-1}$	212.1/25

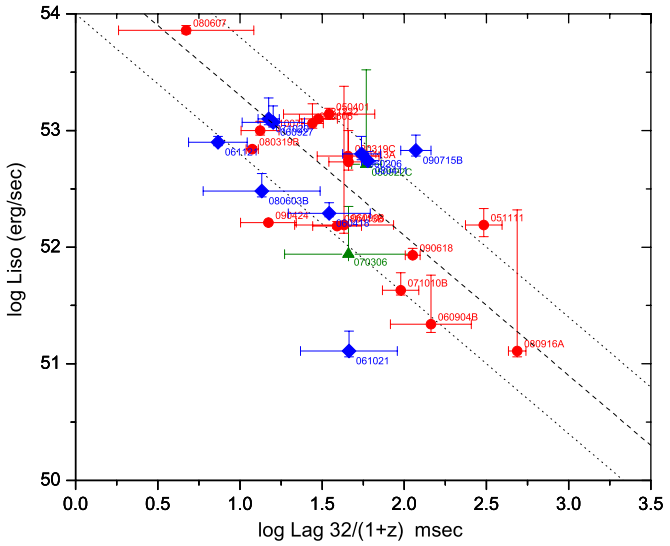

Figure 7. Isotropic luminosity as a function of spectral lag between BAT channels 3 (50–100 keV) and 2 (25–50 keV). The "Gold," "Silver," and "Bronze" samples are represented with red circles, blue diamonds, and green triangles, respectively.

(A color version of this figure is available in the online journal.)

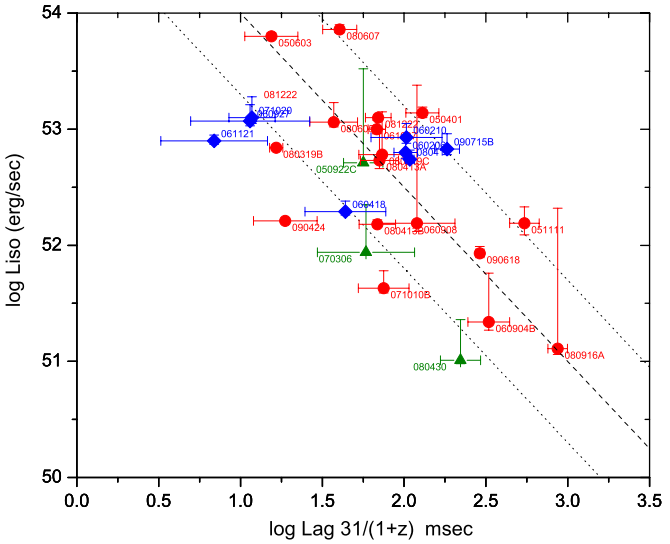

Figure 8. Isotropic luminosity as a function of spectral lag between BAT channels 3 (50–100 keV) and 1 (15–25 keV). The "Gold," "Silver," and "Bronze" samples are represented with red circles, blue diamonds, and green triangles, respectively.

(A color version of this figure is available in the online journal.)

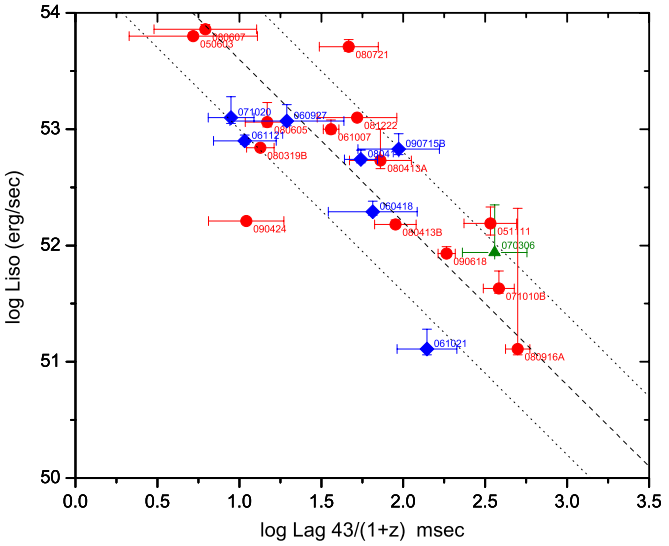

Figure 9. Isotropic luminosity as a function of spectral lag between BAT channels 4 (100–200 keV) and 3 (50–100 keV). The "Gold," "Silver," and "Bronze" samples are represented with red circles, blue diamonds, and green triangles, respectively.

(A color version of this figure is available in the online journal.)

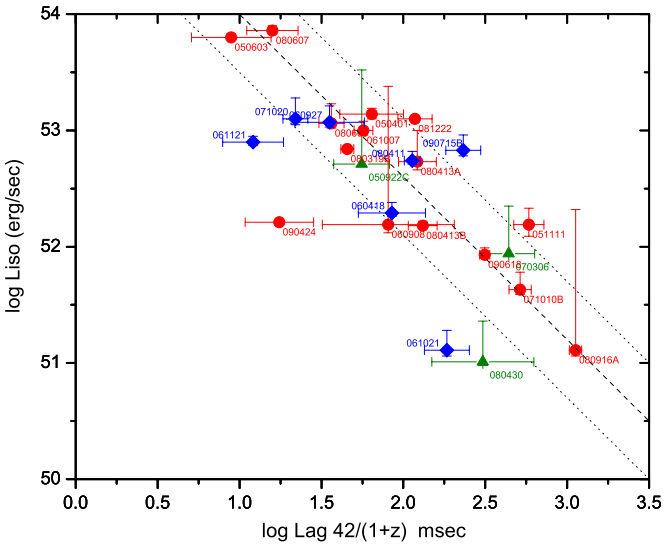

Figure 10. Isotropic luminosity as a function of spectral lag between BAT channels 4 (100–200 keV) and 2 (25–50 keV). The "Gold," "Silver," and "Bronze" samples are represented with red circles, blue diamonds, and green triangles, respectively.

(A color version of this figure is available in the online journal.)

for the time dilation effect (z-correction), and (2) take into account the fact that for GRBs with various redshifts, observed energy bands correspond to different energy bands at the GRB rest frame (k-correction). Gehrels et al. (2006) approximately corrected observed spectral lag for the above-mentioned effects. We also examined these corrections. The z-correction is done by multiplying the lag value by $(1 + z)^{-1}$. The k-correction is approximately done by multiplying the lag value by $(1 + z)^{0.33}$ (Gehrels et al. 2006; Zhang et al. 2009). In Table 5, we list the correlation coefficients with no correction, only z-correction, only k-correction, and both corrections applied. For example, correlation coefficient of Lag31 and $L_{\rm iso}$ is -0.38 without any corrections. After the k-correction the correlation coefficient is -0.29. Therefore, we do not gain a significant improvement in the correlation by applying the k-correction. However, the correlation improves significantly after the z-correction (-0.60). The approximate k-correction of Gehrels et al. (2006) is based on the assumption that the spectral lag is proportional to the pulse width and pulse width is proportional to the energy (Zhang et al. 2009; Fenimore et al. 1995). These approximations depend on clearly identifying a pulse in the light curve and may be of limited validity for multi-pulse structures. A better method would be to define two energy bands in the GRB rest frame and project those two bands into the observer frame and extract lags between them (T. N. Ukwatta, et al. 2010 in preparation).

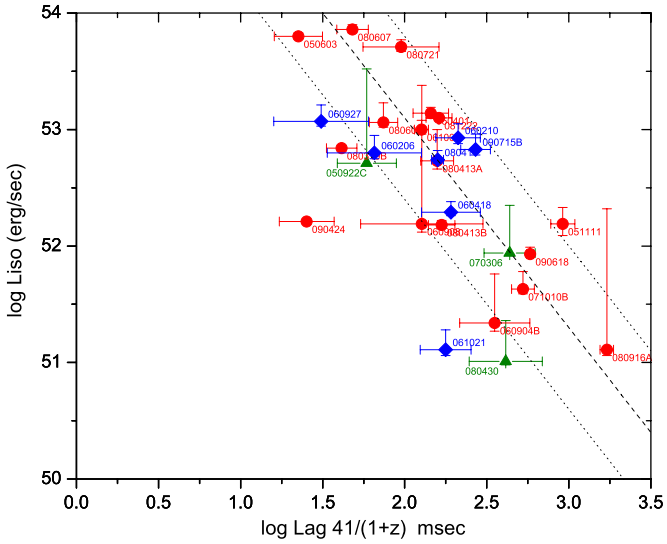

Figure 11. Isotropic luminosity as a function of spectral lag between BAT channels 4 (100–200 keV) and 1 (15–25 keV). The "Gold," "Silver," and "Bronze" samples are represented with red circles, blue diamonds, and green triangles, respectively.

(A color version of this figure is available in the online journal.)

Table 5
Correlation Coefficients with Various Corrections

Channels	No Correction	z-Correction	k-Correction	Both Corrections
Channel 21	−0.38	−0.63	−0.29	−0.55
Channel 32	−0.43	−0.66	−0.33	−0.60
Channel 31	−0.39	−0.60	−0.31	−0.54
Channel 43	−0.61	−0.77	−0.54	−0.73
Channel 42	−0.58	−0.75	−0.51	−0.71
Channel 41	−0.43	−0.67	−0.32	−0.61

5. CONCLUSION

In this work, we have used the CCF technique to extract spectral lags for a sample of *Swift* BAT GRBs with known redshifts. By using Monte Carlo simulations, we have extended this technique to reliably determine the uncertainties in the extracted spectral lags. Normally these uncertainties would be very difficult to calculate analytically.

This study provides further support for the existence of the lag–luminosity correlation, originally proposed by Norris et al. (2000). We note however that there is a significant scatter in the correlation.

The authors are indebted to the late Dr. David L. Band for fruitful and insightful discussions on the CCF methodology. In addition, we take this opportunity to acknowledge useful input from David A. Kahn regarding the luminosity calculations. We also thank the anonymous referee for comments and suggestions that significantly improved the paper. The NASA grant NNX08AR44A provided partial support for this work and is gratefully acknowledged.

REFERENCES

Band, D. L. 1997, ApJ, 486, 928
Band, D. L., Norris, J. P., & Bonnell, J. T. 2004, ApJ, 613, 484
Band, D., et al. 1993, ApJ, 413, 281
Barthelmy, S. D., et al. 2005, Space Sci. Rev., 120, 143
Barthelmy, S. D., et al. 2008, GRB Coordinates Network, 7606, 1
Berger, E., & Becker, G. 2005, GRB Coordinates Network, 3520, 1
Bissaldi, E., & McBreen, S. 2008, GRB Coordinates Network, 8715, 1
Bloom, J. S., Frail, D. A., & Kulkarni, S. R. 2003, ApJ, 594, 674
Cannizzo, J. K., Ukwatta, T. N., Palmer, D. M., Margutti, R., & de Pasquale, M. 2009, GCN Report, 221, 1
Cenko, S. B., Cucchiara, A., Fox, D. B., Berger, E., & Price, P. A. 2007, GRB Coordinates Network, 6888, 1
Cenko, S. B., et al. 2009, GRB Coordinates Network, 9518, 1
Chen, L., Lou, Y.-Q., Wu, M., Qu, J.-L., Jia, S.-M., & Yang, X.-J. 2005, ApJ, 619, 983
Cheng, L. X., Ma, Y. Q., Cheng, K. S., Lu, T., & Zhou, Y. Y. 1995, A&A, 300, 746
Chornock, R., Perley, D. A., Cenko, S. B., & Bloom, J. S. 2009, GRB Coordinates Network, 9243, 1
Connaughton, V. 2009, GRB Coordinates Network, 9230, 1
Cucchiara, A., & Fox, D. B. 2008, GRB Coordinates Network, 7654, 1
Cucchiara, A., Fox, D. B., Cenko, S. B., & Berger, E. 2008, GRB Coordinates Network, 8713, 1
D'Elia, V., et al. 2009, ApJ, 694, 332
Donaghy, T. Q., et al. 2006, arXiv:astro-ph/0605570
Fenimore, E. E., in't Zand, J. J. M., Norris, J. P., Bonnell, J. T., & Nemiroff, R. J. 1995, ApJ, 448, L101
Fynbo, J. P. U., et al. 2009, ApJS, 185, 526 (erratum: ApJS, 186, 485)
Gaskell, C. M., & Peterson, B. M. 1987, ApJS, 65, 1
Gehrels, N., et al. 2004, ApJ, 611, 1005
Gehrels, N., et al. 2006, Nature, 444, 1044
Golenetskii, S., Aptekar, R., Mazets, E., Pal'Shin, V., Frederiks, D., & Cline, T. 2005a, GRB Coordinates Network, 3518, 1
Golenetskii, S., Aptekar, R., Mazets, E., Pal'Shin, V., Frederiks, D., & Cline, T. 2005b, GRB Coordinates Network, 3179, 1
Golenetskii, S., Aptekar, R., Mazets, E., Pal'Shin, V., Frederiks, D., & Cline, T. 2006a, GRB Coordinates Network, 5748, 1
Golenetskii, S., Aptekar, R., Mazets, E., Pal'Shin, V., Frederiks, D., & Cline, T. 2006b, GRB Coordinates Network, 5837, 1
Golenetskii, S., Aptekar, R., Mazets, E., Pal'Shin, V., Frederiks, D., & Cline, T. 2006c, GRB Coordinates Network, 5722, 1
Golenetskii, S., Aptekar, R., Mazets, E., Pal'Shin, V., Frederiks, D., & Cline, T. 2007a, GRB Coordinates Network, 6960, 1
Golenetskii, S., Aptekar, R., Mazets, E., Pal'Shin, V., Frederiks, D., & Cline, T. 2007b, GRB Coordinates Network, 6879, 1
Golenetskii, S., Aptekar, R., Mazets, E., Pal'Shin, V., Frederiks, D., & Cline, T. 2008a, GRB Coordinates Network, 7487, 1
Golenetskii, S., Aptekar, R., Mazets, E., Pal'Shin, V., Frederiks, D., & Cline, T. 2008b, GRB Coordinates Network, 7854, 1
Golenetskii, S., Aptekar, R., Mazets, E., Pal'Shin, V., Frederiks, D., & Cline, T. 2008c, GRB Coordinates Network, 7589, 1
Golenetskii, S., Aptekar, R., Mazets, E., Pal'Shin, V., Frederiks, D., & Cline, T. 2008d, GRB Coordinates Network, 7482, 1
Golenetskii, S., Aptekar, R., Mazets, E., Pal'Shin, V., Frederiks, D., Ulanov, M., & Cline, T. 2006d, GRB Coordinates Network, 4989, 1
Golenetskii, S., et al. 2008e, GRB Coordinates Network, 7862, 1
Golenetskii, S., et al. 2008f, GRB Coordinates Network, 7995, 1
Golenetskii, S., et al. 2009, GRB Coordinates Network, 9679, 1
Grupe, D., et al. 2009, GCN Report, 190, 1
Guidorzi, C., Stamatikos, M., Landsman, W., Barthelmy, S. D., Burrows, D. N., Roming, P., & Gehrels, N. 2008, GCN Report, 139, 1
Hakkila, J., Giblin, T. W., Norris, J. P., Fragile, P. C., & Bonnell, J. T. 2008, ApJ, 677, L81
Hakkila, J., et al. 2007, ApJS, 169, 62
Holland, S. T., et al. 2007, GCN Report, 94, 2
Ioka, K., & Nakamura, T. 2001, ApJ, 554, L163
Jakobsson, P., Vreeswijk, P. M., Hjorth, J., Malesani, D., Fynbo, J. P. U., & Thoene, C. C. 2007, GRB Coordinates Network, 6952, 1
Jaunsen, A. O., et al. 2008, ApJ, 681, 453
Kaneko, Y., Preece, R. D., Briggs, M. S., Paciesas, W. S., Meegan, C. A., & Band, D. L. 2006, ApJS, 166, 298
Komatsu, E., et al. 2009, ApJS, 180, 330
Kouveliotou, C., Meegan, C. A., Fishman, G. J., Bhat, N. P., Briggs, M. S., Koshut, T. M., Paciesas, W. S., & Pendleton, G. N. 1993, ApJ, 413, L101
Krimm, H. A., et al. 2009, ApJ, 704, 1405
Li, T.-P., Qu, J.-L., Feng, H., Song, L.-M., Ding, G.-Q., & Chen, L. 2004, Chin. J. Astron. Astrophys., 4, 583
Liang, N., Xiao, W. K., Liu, Y., & Zhang, S. N. 2008, ApJ, 685, 354
Lu, R.-J., Qin, Y.-P., Zhang, Z.-B., & Yi, T.-F. 2006, MNRAS, 367, 275
Mangano, V., Cummings, J., Barthelmy, S. D., Sbarufatti, B., Schady, P., Burrows, D. N., Roming, P., & Gehrels, N. 2008, GCN Report, 147, 1
Mangano, V., et al. 2008, GCN Report, 144, 1

Markwardt, C., Kennea, J., Mangano, V., Barthelmy, S. D., Burrows, D. N., Roming, P., & Gehrels, N. 2007, GCN Report, 92, 1
Marshall, F. E., Barthelmy, S. D., Burrows, D. N., Evans, P. A., Oates, S. R., Stamatikos, M., & Gehrels, N. 2008, GCN Report, 129, 1
Marshall, F. E., Guidorzi, C., Ward, P. A., Barthelmy, S. D., Burrows, D. N., Roming, P., & Gehrels, N. 2008, GCN Report, 156, 1
McBreen, S., et al. 2009, GRB Coordinates Network, 9535, 1
Mosquera Cuesta, H. J., Turcati, R., Furlanetto, C., Khachatryan, H. G., Mirzoyan, S., & Yegorian, G. 2008, A&A, 487, 47
Murakami, T., Yonetoku, D., Izawa, H., & Ioka, K. 2003, PASJ, 55, L65
Norris, J. P. 1995, Ap&SS, 231, 95
Norris, J. P. 2002, ApJ, 579, 386
Norris, J. P., & Bonnell, J. T. 2006, ApJ, 643, 266
Norris, J. P., Bonnell, J. T., Kazanas, D., Scargle, J. D., Hakkila, J., & Giblin, T. W. 2005, ApJ, 627, 324
Norris, J. P., Marani, G. F., & Bonnell, J. T. 2000, ApJ, 534, 248
Norris, J. P., Nemiroff, R. J., Bonnell, J. T., Scargle, J. D., Kouveliotou, C., Paciesas, W. S., Meegan, C. A., & Fishman, G. J. 1996, ApJ, 459, 393
Palmer, D., et al. 2006, GRB Coordinates Network, 4697, 1
Penprase, B. E., et al. 2006, ApJ, 646, 358
Piranomonte, S., et al. 2008, A&A, 492, 775
Prochaska, J. X., Chen, H.-W., Bloom, J. S., Falco, E., & Dupree, A. K. 2006, GRB Coordinates Network, 5002, 1
Prochaska, J. X., et al. 2009, ApJ, 691, L27
Qin, Y.-P., Zhang, Z.-B., Zhang, F.-W., & Cui, X.-H. 2004, ApJ, 617, 439
Racusin, J. L., Holland, S. T., Cummings, J., Oates, S. R., & Schady, P. 2008, GCN Report, 134, 1
Ryde, F. 2005, A&A, 429, 869
Sakamoto, T., et al. 2008, ApJS, 175, 179
Sakamoto, T., et al. 2009, ApJ, 693, 922
Salmonson, J. D. 2000, ApJ, 544, L115
Salmonson, J. D., & Galama, T. J. 2002, ApJ, 569, 682
Sato, G., et al. 2008, GRB Coordinates Network, 7591, 1
Sbarufatti, B., et al. 2008, GCN Report, 142, 1
Schady, P., Baumgartner, W. H., & Beardmore, A. P. 2009, GCN Report, 232, 1
Schaefer, B. E. 2004, ApJ, 602, 306
Schaefer, B. E. 2007, ApJ, 660, 16
Shen, R.-F., Song, L.-M., & Li, Z. 2005, MNRAS, 362, 59
Stamatikos, M., Ukwatta, T. N., Sakamoto, T., Barthelmy, S. D., Norris, J. P., Gehrels, N., & Dhuga, K. S. 2008a, in AIP Conf. Ser. 1000, Gamma-ray Bursts 2007: Proceedings of the Santa Fe Conf., ed. M. Galassi, D. Palmer, & E. Fenimore (Melville, NY: AIP), 137
Stamatikos, M., et al. 2008b, GRB Coordinates Network, 7483, 1
Stamatikos, M., et al. 2009, in AIP Conf. Ser. 1133, Gamma-ray Burst: Sixth Huntsville Symp., ed. C. Meegan, N. Gehrels, & C. Kouveliotou (Melville, NY: AIP), 356
Tsutsui, R., Nakamura, T., Yonetoku, D., Murakami, T., Tanabe, S., & Kodama, Y. 2008, MNRAS, 386, L33
Vetere, L., Cummings, J. R., Breeveld, A., Barthelmy, S. D., Burrows, D. N., Roming, P. W. A., & Gehrels, N. 2009, GCN Report, 236, 1
Watson, D., et al. 2006, ApJ, 652, 1011
Wiersema, K., et al. 2009, GRB Coordinates Network, 9673, 1
Wu, B., & Fenimore, E. 2000, ApJ, 535, L29
Zhang, B., et al. 2009, ApJ, 703, 1696
Ziaeepour, H., Oates, S., Sakamoto, T., Baumgartner, W., Starling, R. L. C., & Holland, S. T. 2008, GCN Report, 167, 3